Emergence of charge-4e superconductivity from 2D nematic superconductors

Xuan Zou, ¹ Zhou-Quan Wan, ² and Hong Yao^{1,*}

¹Institute for Advanced Study, Tsinghua University, Beijing 100084, China ²Center for Computational Quantum Physics, Flatiron Institute, New York, NY, 10010, USA (Dated: October 31, 2025)

Charge-4e superconductivity is an exotic state of matter that may emerge as a vestigial order from a charge-2e superconductor with multicomponent superconducting order parameters. Showing its emergence in a microscopic model from numerically-exact large-scale computations has been rare so far. Here, we propose a microscopic lattice model with a nematic superconducting ground state and show that it supports a rich set of vestigial phases at elevated temperature, including a charge-4e phase and a quasi-long-range nematic phase, by performing large-scale Monte Carlo simulations. Combining theoretical analysis with Monte Carlo simulations, we uncover the nature of these phases and show that the phase transitions are governed by the proliferation of distinct topological defects: half superconducting vortices, $(\frac{1}{2}, \frac{1}{2})$ vortices, integer nematic vortices, and domain-wall excitations. In particular, we demonstrate that domain-wall proliferation is crucial for the quasi-nematic phase and should be carefully accounted for in phase transitions associated with vestigial charge-4e order.

Introduction.—Since the Bardeen-Cooper-Schrieffer (BCS) theory [1] was established as the microscopic foundation of conventional superconductivity, understanding unconventional superconductors has remained a central challenge in condensed matter physics. In usual superconductors, superconductivity arises from the phase coherence of charge-2e Cooper pairs. However, it is also possible to form charge-4e superconductivity by condensing electron quartets that consist of four electrons [2] (Similar quarteting mechanism has been discussed in nuclear matter [3].). As a novel state of matter, charge-4e superconductivity has gained increasing attention in recent years [4–34]. This exotic state of matter is inherently strongly correlated; even its mean-field Hamiltonian remains an interacting theory [13], making it an intriguing topic for study. Despite recent experimental progress [35], the identification of charge-4e order in real materials remains rare, and many of its fundamental properties remain unresolved.

For 2D charge-2e superconductors, phase fluctuations of superconducting (SC) order are described by the XY model, where a direct transition between a charge-2e SC and normal state occurs at the Berezinskii-Kosterlitz-Thouless (BKT) transition via vortex proliferation [36– 38]. However, for a generalized XY model, a charge-4e state may arise when half-vortices could play a similar role as normal vortices [39, 40]. At sufficiently low temperatures, half-vortices are bound by string-like domainwall defects. When the temperature becomes comparable to the string tension, an Ising transition from charge-2eto charge-4e order occurs. At higher temperatures, the proliferation of half-vortices disrupts the charge-4e phase. This mechanism has been corroborated by field-theoretic analyses, Monte Carlo simulations, and tensor-network calculations [41–49].

Alternatively, charge-4e superconductivity was proposed to arise from SC states with additional broken symmetries, including pair-density-wave (PDW) order [9, 50–

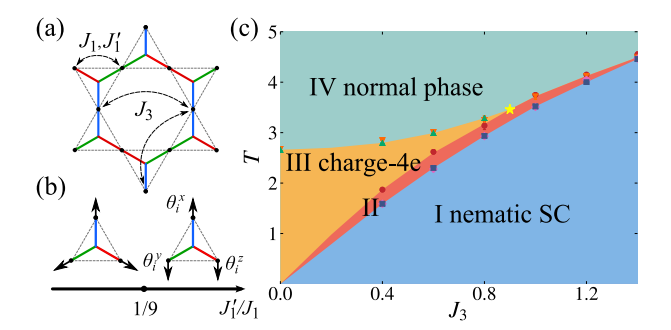


FIG. 1. (a) Honeycomb lattice with fields θ_i residing on the bonds and Josephson couplings J_1 , J_1' , and J_3 . (b) Groundstate configurations for different ratios of J_1'/J_1 . (c) Phase diagram of the generalized XY model with $J_1 = 1$ and $J_1' = 3.2$. The yellow star (J_3^*, T^*) marks the tricritical point. Phase I: nematic SC state with charge-2e QLRO and nematic LRO; Phase II: restoration of discrete rotational symmetry leading to a quasi-long-range nematic phase; Phase III: charge-4e QLRO without nematicity; Phase IV: disordered phase. Colored points denote transition points obtained from different physical observables [61].

56] and nematic superconductors [57–60]. In these cases, charge-4e order can appear as a vestigial phase when the additional broken symmetry is restored first, with transitions mediated by topological defects such as double dislocations [9, 14, 50] or nematic vortices [15, 16]. Several studies of the phase diagram have been conducted using renormalization group analysis and numerical simulations [15–17, 20]. Nevertheless, the interplay between the domain-wall excitations and point-like topological defects in these melting scenarios has received comparatively little attention. Since such string-like domain-wall defects can strongly influence the stability of intermediate phases, their contribution requires further theoretical clarification.

In this paper, we propose a generalized XY model

whose ground state simultaneously breaks U(1) symmetry and lattice rotational symmetry, realizing a nematic superconductor. Consistent with earlier studies [15, 16], a charge-4e phase emerges upon heating. However, our Monte Carlo simulations and theoretical analysis reveal a qualitatively new phase diagram, featuring an intermediate quasi-long-range nematic phase between the nematic SC and charge-4e states. The appearance of the quasi-nematic order is intriguing, as it contrasts with the conventional expectation that discrete C_2 or C_3 latticerotational symmetry breaking in two dimensions can only produce true long-range nematicity, with exceptions proposed in quasicrystals [60] and twisted bilayer systems [62]. In our model, the emergence of the quasi-long-range nematic phase originates from domain-wall excitations, demonstrating that both string-type and vortex-type defects are essential for a complete description of charge-4e melting transitions.

The model.—We consider a generalized XY model with U(1) phase fields θ_i living on the bonds of a honeycomb lattice, as illustrated in Fig. 1(a). The Hamiltonian is defined as follows:

$$H = J_1 \sum_{\langle i,j \rangle} \cos(\theta_i - \theta_j) - J_1' \sum_{\langle i,j \rangle} \cos(2\theta_i - 2\theta_j) - J_3 \sum_{\langle i,j \rangle'} \cos(\theta_i - \theta_j),$$
(1)

with $0 \leq \theta_i < 2\pi$. Here, J_1 and J_1' denote nearest-neighbor couplings, and J_3 denotes the third-nearest-neighbor coupling. Throughout, we assume $J_1, J_1', J_3 > 0$; weak next-nearest-neighbor couplings are omitted, as they do not qualitatively alter the phase diagram. The model respects several symmetries: global U(1) rotations $(\theta_i \to \theta_i + \delta\theta)$, time reversal $(\theta_i \to -\theta_i)$, lattice translations, and C_3 rotational symmetry.

The ground state of this system can be determined straightforwardly. The honeycomb lattice is divided into three types of bonds, indicated by different colors in Fig. 1(a), which are connected by J_3 couplings without frustration. The ground state is therefore obtained by minimizing the energy within a single triangle, yielding a 120° state for $J'_1 < J_1/9$ and a nematic state for $J'_1 > J_1/9$, as illustrated in Fig. 1(b). In this work we focus on the latter case. This ground state preserves time-reversal symmetry but breaks both U(1) and lattice rotational symmetries, and can thus be regarded as a nematic SC state.

To study the finite-temperature behavior, we performed Monte Carlo simulations to obtain the phase diagram shown in Fig. 1(c). Upon heating, the uniform SC order, i.e., charge-2e quasi-long-range order (QLRO), is first destroyed at $T_{\rm dw}$ (phase I \rightarrow II), while the nematic long-range order (LRO) simultaneously reduces to QLRO. At higher temperatures, two distinct transition sequences appear, separated by a tricritical point J_3^* . For

 $0 < J_3 < J_3^*$, nematic QLRO vanishes at $T_{\rm nem}$ (phase II \rightarrow III), followed by the loss of charge-4e QLRO at T_{4e} (phase III \rightarrow IV). In contrast, for $J_3 > J_3^*$, the simulations indicate a direct transition from phase II to IV, in which all orders are destroyed simultaneously. In the next section, we analyze the topological defects of the model to account for the transition behaviors observed in Fig. 1(c).

Effective theory.—Deep in the nematic superconducting phase, amplitude fluctuations of the order parameters can be neglected. The model described in Eq. (1) can be characterized by the following order parameters:

$$\Delta_{0}(\mathbf{r}) \sim e^{i\theta_{\mathbf{r}}^{x}} + e^{i\theta_{\mathbf{r}}^{y}} + e^{i\theta_{\mathbf{r}}^{z}},
\Delta_{+}(\mathbf{r}) \sim e^{i\theta_{\mathbf{r}}^{x}} + e^{i\left(\frac{2\pi}{3} + \theta_{\mathbf{r}}^{y}\right)} + e^{i\left(\frac{4\pi}{3} + \theta_{\mathbf{r}}^{z}\right)},
\Delta_{-}(\mathbf{r}) \sim e^{i\theta_{\mathbf{r}}^{x}} + e^{i\left(-\frac{2\pi}{3} + \theta_{\mathbf{r}}^{y}\right)} + e^{i\left(-\frac{4\pi}{3} + \theta_{\mathbf{r}}^{z}\right)},$$
(2)

where Δ_0 denotes the uniform SC component and Δ_{\pm} represent nematic SC order parameters. These order parameters transform under U(1) rotations as $\Delta_0 \to \Delta_0 e^{i\delta\theta}$ and $\Delta_{\pm} \to \Delta_{\pm} e^{i\delta\theta}$, and under C_3 lattice rotations as $\Delta_0 \to \Delta_0$ and $\Delta_{\pm} \to \Delta_{\pm} e^{\pm i2\pi/3}$.

Neglecting amplitude fluctuations, we parametrize the order parameters as $\Delta_0(\mathbf{r}) = |\Delta_0|e^{i\theta_0(\mathbf{r})}$, $\Delta_{\pm}(\mathbf{r}) = |\Delta_{\pm}|e^{i[\theta(\mathbf{r})\pm\phi(\mathbf{r})]}$. From these we identify the charge-4e order, $\Delta_{4e}(\mathbf{r}) = \Delta_{+}\Delta_{-} = |\Delta_{4e}|e^{i2\theta(\mathbf{r})}$, and the nematic order, $Q(\mathbf{r}) = \Delta_{+}\Delta_{-}^{\dagger} = |Q|e^{i2\phi(\mathbf{r})}$.

The corresponding effective Hamiltonian density reads

$$H = \frac{\rho}{2T} (\nabla \theta)^2 + \frac{\rho_0}{2T} (\nabla \theta_0)^2 - g \cos(2\theta_0 - 2\theta) + \frac{\kappa}{2T} (\nabla \phi)^2 - g_3 \cos(\theta_0 - \theta) \cos(3\phi),$$
(3)

where ρ and ρ_0 are the superfluid stiffnesses, g couples the uniform and nematic SC phases, κ is the nematic stiffness, and g_3 encodes the lowest-order anisotropy allowed by symmetry. Gauge invariance under $(\theta, \phi) \rightarrow (\theta + \pi, \phi + \pi)$ forbids terms such as $\tilde{g}_3 \cos(3\phi)$. In the absence of θ_0 , this Hamiltonian reduces to that of Refs. [9, 15]. The g term originates from the coupling $\Delta_0^2(\Delta_+\Delta_-)^* + \text{h.c.}$, while the g_3 term has the form $\Delta_0\Delta_+(\Delta_-^*)^2 + \Delta_0\Delta_-(\Delta_+^*)^2 + \text{h.c.}$. As we will show, the g and g_3 terms play a central role in the emergence of quasi-nematicity.

More generally, if the symmetry transformation is $\Delta_{\pm} \to e^{\pm i 2\pi/q} \Delta_{\pm}$ with $q \neq 3$, the g_3 term is forbidden. In that case, the leading coupling between the uniform and nematic SC components reduces to $\Delta_0^2 (\Delta_+ \Delta_-)^* + \text{h.c.} \sim \cos(2\theta_0 - 2\theta)$. This term alone can drive an Ising transition between charge-2e and charge-4e phases, accompanied by the disappearance of the uniform SC order. A similar analysis also applies to the coupling between the uniform SC and PDW states [61].

To clarify the origin of the phase boundaries in our phase diagram, we first consider the region where the uniform superconducting component is disordered (T >

 $T_{\rm dw}$). In this region, the topological defects can be systematically described by switching to the dual boson variables $\tilde{\theta}$ and $\tilde{\phi}$. The corresponding dual Hamiltonian density takes the form [9, 15]

$$\tilde{H} = \frac{T}{2\rho} (\partial \tilde{\theta})^2 + \frac{T}{2\kappa} (\partial \tilde{\phi})^2 - g_{1,0} \cos 2\pi \tilde{\theta} - g_{0,1} \cos 2\pi \tilde{\phi} - g_{\frac{1}{2},\frac{1}{2}} \cos \pi \tilde{\theta} \cos \pi \tilde{\phi}.$$
(4)

where $g_{1,0}, g_{0,1}$, and $g_{\frac{1}{2},\frac{1}{2}}$ characterize the strength of different topological defects: integer SC vortices, integer nematic vortices, and $(\frac{1}{2},\frac{1}{2})$ vortices. These defects correspond to different windings of the phase fields: SC (nematic) vortices involve 2π windings of θ (ϕ), with energies $\pi \rho \log L$ and $\pi \kappa \log L$, respectively. In addition, because the order parameters Δ_{\pm} are invariant under the discrete transformation $(\theta,\phi) \to (\theta+\pi,\phi+\pi)$, a $(\frac{1}{2},\frac{1}{2})$ vortex is also allowed, carrying π windings in both fields and energy $\frac{\pi}{4}(\rho+\kappa) \log L$.

The competition among these vortex species dictates the phase diagram: from the dual perspective, the sequence of transitions is determined by which vortex type proliferates first. When $\kappa/\rho < 1/3$, nematic vortices proliferate and destroy nematic order, yielding a charge-4e superconductor. Upon further heating, half SC vortices proliferate and drive the loss of charge-4e order [63]. For κ/ρ slightly above 1/3, proliferation of $(\frac{1}{2},\frac{1}{2})$ vortices instead produces a direct transition in which nematic and SC orders vanish simultaneously.

In our model parameters, J_3 is proportional to κ , so increasing J_3 raises κ/ρ . This explains the phase-boundary structure in Fig. 1(c): for $J_3 < J_3^*$, the system undergoes successive transitions (phase II \to III \to IV), whereas for $J_3 > J_3^*$, nematic and charge-4e orders disappear together in a single transition (phase II \to IV). These results are fully consistent with the predictions of the dual Hamiltonian in Eq. (4).

However, this reduced model alone cannot explain the emergence of the quasi-nematic phase (phase II) observed in the full phase diagram. To capture this feature, we need to include the uniform superconducting field θ_0 and analyze how its coupling to θ and ϕ reshapes the phase structure.

Quasi-nematic phase.—In general, the uniform SC component Δ_0 can coexist with multi-component SC states. Experimentally, Δ_0 is often observed together with, and in some cases even dominating over, states such as PDW order [64–66]. For Z_2 -broken nematic superconductivity and incommensurate unidirectional PDW states, the leading coupling between Δ_0 and the multi-component SC fields Δ_{\pm} takes the form $\Delta_0^2(\Delta_+\Delta_-)^* + \text{h.c.} \sim \cos(2\theta_0 - 2\theta)$. In this case, the transition that disorders the uniform SC state belongs to the Ising universality class, driven by the proliferation of domain walls.

The mechanism for the charge-2e to charge-4e transition via proliferation of Ising-type domain walls has been

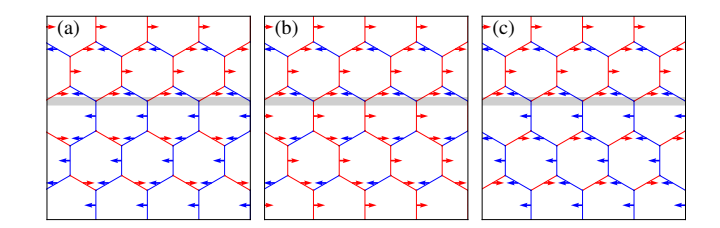


FIG. 2. Demonstration of different domains with a length of 4 units. The values of $(\theta^x, \theta^y, \theta^z)$ are $(0,0,\pi)$ in the upper part, and (a) $(\pi,\pi,0)$, (b) $(0,\pi,0)$, and (c) $(\pi,0,\pi)$ below the domain wall (the shaded region). The energy cost of the domain wall increases with its length and is proportional to $6J_3$, $4J_3$, and $2J_3$ for cases (a), (b), and (c), respectively.

studied in generalized XY models [39, 40]. In our model, several types of domain walls appear, as illustrated in Fig. 2. Domain wall (a) is of Ising type and induces a π shift in the fields $(\theta_0, \theta) \to (\theta_0 + \pi, \theta + \pi)$. Domain wall (b) rotates the nematic field by $2\pi/3$, $\phi \to \phi + 2\pi/3$. Domain wall (c) combines these effects, inducing $(\theta_0, \theta) \to (\theta_0 + \pi, \theta + \pi, \phi \to \phi + 2\pi/3)$, or equivalently $(\theta_0 \to \theta_0 + \pi, \theta \to \theta, \phi \to \phi + \pi/3)$. Among these, type-(c) has the lowest energy cost, and its proliferation drives the system into the quasi-nematic phase.

Specifically, at the temperature $T_{\rm dw}$, the proliferation of type-(c) domain walls disorders the uniform charge-2e condensate, $\langle e^{i\theta_0} \rangle \simeq 0$, rendering the anisotropic coupling g_3 irrelevant. The remaining leading anisotropy is the $\cos(6\phi)$ term, which becomes irrelevant at $T \sim 4T_{\rm nem}/9$, a scale lower than $T_{\rm dw}$. As a result, the system directly enters a quasi-long-range nematic phase.

In the following section, we present Monte Carlo simulations that provide direct evidence supporting this mechanism and the phase transitions summarized in Fig. 1.

Monte Carlo results.—To study the critical behavior and phase diagram, we performed Monte Carlo simulations using the cluster algorithm [67, 68], with $J_1' = 3.2$, $J_1 = 1.0$, and varying J_3 to obtain the finite-temperature phase diagram in Fig. 1. The uniform charge-2e order parameter is $\Delta_{2e}(\mathbf{r}_i) = e^{i\theta_i^x} + e^{i\theta_i^y} + e^{i\theta_i^z}$, with structure factor $S_{2e}(\mathbf{q}, L) = \frac{1}{3L^2} \left\langle \left| \sum_i \Delta_{2e}(\mathbf{r}_i) e^{i\mathbf{q}\cdot\mathbf{r}_i} \right|^2 \right\rangle$. Transition points were located using the Binder cumulant and RG-invariant ratio,

$$U_{2e} = 2 - \frac{\langle |\sum_{i} \Delta_{2e}(\mathbf{r}_{i})|^{4} \rangle}{\langle |\sum_{i} \Delta_{2e}(\mathbf{r}_{i})|^{2} \rangle^{2}}, \quad R_{2e} = 1 - \frac{S_{2e}(\delta \mathbf{q}, L)}{S_{2e}(0, L)},$$
 (5)

where $\delta \mathbf{q}$ is the smallest momentum on the finite lattice. The charge-4e and nematic order parameters are defined as $\Delta_{4e}(\mathbf{r}_i) = e^{i2\theta_i^x} + e^{i2\theta_i^y} + e^{i2\theta_i^z}$, and $Q(\mathbf{r}_i) = e^{i(\theta_i^y - \theta_i^z)} + e^{i\frac{2\pi}{3}}e^{i(\theta_i^x - \theta_i^y)} + e^{i\frac{4\pi}{3}}e^{i(\theta_i^z - \theta_i^x)}$, with Binder cumulants and RG ratios defined analogously to Eq. (5).

In general, the crossing of dimensionless quantities such as Binder cumulants and RG-invariant ratios sig-

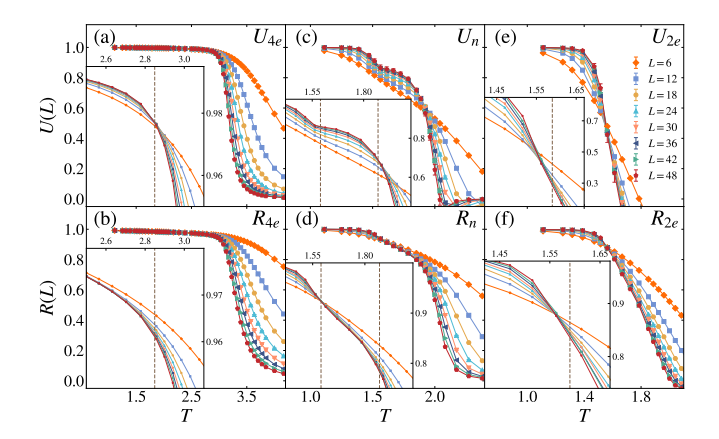


FIG. 3. The plot of Binder cumulants U(L) and the RG-invariant ratio R(L) for the different orders at $J_3=0.4$. The insets depict a close-up view of the transition points. (a)-(b) correspond to the charge-4e order, where the dashed line denotes the transition temperature $T_{4e}=2.849$. (c)-(d) represent the nematic order, where the dashed lines denote the transition temperatures $T_{\rm nem}=1.87$ and $T'_{\rm nem}\simeq T_{\rm dw}=1.59$. (e)-(f) show the charge-2e order, where the dashed line denotes the transition temperature $T_{\rm dw}=1.59$.

nals critical points, as these quantities approach unity in the ordered phase and vanish in the disordered phase with increasing system size [69]. For systems with QLRO, however, the behavior can differ: in a BKT phase, one may still observe crossings, but more characteristically, the curves for different system sizes collapse onto each other, separating only at the transition to the disordered phase.

Fig. 3 shows the behavior of Binder cumulants and the RG-invariant ratios of different order parameters for $J_3 = 0.4$, with similar behavior at $J_3 = 1.2$ [61]. For charge-4e order, the curves collapse below T_{4e} and separate above it, consistent with QLRO [Fig. 3(a-b)]. For charge-2e order, a crossing at $T_{\rm dw}$ signals the loss of uniform superconductivity [Fig. 3(e-f)]. For nematic order, Binder cumulants and RG ratios cross at distinct points: they saturate near unity below $T'_{\rm nem}$, vanish above $T_{\rm nem}$, and remain finite in the window $T'_{\rm nem} < T < T_{\rm nem}$, revealing an intermediate quasi-nematic phase [Fig. 3(c-d)].

The transition temperatures T_{4e} , $T_{\rm dw}$, $T_{\rm nem}$, and $T'_{\rm nem}$ were determined by finite-size extrapolation of the crossing points of U_{4e} , U_{2e} , U_n , and R_n , respectively. For all the J_3 values that we simulate in this paper, the transition temperature $T'_{\rm nem}$ coincides with $T_{\rm dw}$ within the numerical errors [61], as expected. Furthermore, for $J_3 \gtrsim 1.0$, T_{4e} coincides with $T_{\rm nem}$, demonstrating the simultaneous destruction of the charge-4e and the nematic QLRO. These results point to a tricritical point J_3^* that separates the two distinct transition sequences summarized in Fig. 1.

To identify which vortices proliferate and to determine the charge-4e transition more precisely, we compute the

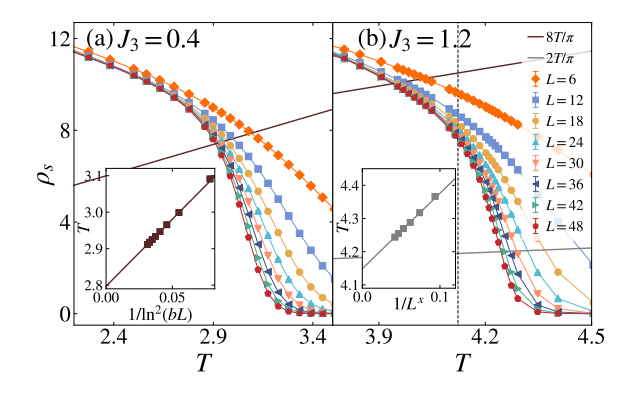


FIG. 4. (a). The size-dependence of spin stiffness ρ for $J_3=0.4$. The straight line is $\rho=8T/\pi$. The inset figure is the finite-size extrapolation of the critical temperature $T^*(L)$ using $T^*(L)=T_{4e}(\infty)+\frac{a}{\ln^2(bL)}$, where $T^*(L)$ is the crossing point with line $\rho=8T/\pi$. (b). The size-dependence of spin stiffness ρ for $J_3=1.2$. The two straight lines are $\rho=8T/\pi$ and $2T/\pi$. The vertical dashed line represents the critical temperature extracted from U_{4e} , indicating a stiffness jump lies between $8T/\pi$ and $2T/\pi$. The inset figure is the finite-size extrapolation of the critical temperature $T^*(L)$ using $T^*(L)=T_{4e}(\infty)+\frac{a}{L^x}$, where $T^*(L)$ is the crossing point with line $\rho=2T/\pi$.

superfluid stiffness $\rho = \partial^2 f(\varphi)/\partial \varphi^2$, where φ is a twist angle and $f(\varphi)$ is the free-energy density [44]. As shown in Fig. 4, ρ exhibits the characteristic finite-size scaling behavior of a universal jump at T_{4e} . For $J_3 < J_3^*$, the jump takes the expected value $8T_{4e}/\pi$, consistent with the proliferation of half-vortices. In Fig. 4(a), the slope of the straight line is $8/\pi$ and the T_{4e} can be extracted using the finite-size scaling form $T^*(L) = T_{4e}(\infty) + a/\ln^2(bL)$ [70, 71]. The fit for $J_3 = 0.4$, shown in the inset of Fig. 4(a), yields a transition temperature consistent with that obtained from U_{4e} [61]. For $J_3 > J_3^*$, the stiffness jump deviates from $8T_{4e}/\pi$. For example, at $J_3 = 1.2$ the jump falls between $8T_{4e}/\pi$ and $2T_{4e}/\pi$ [Fig. 4(b)], consistent with the scenario in which $(\frac{1}{2}, \frac{1}{2})$ vortices proliferate, giving $T_{4e} = \frac{\pi}{8}(\rho + \kappa)$.

To further confirm the two distinct transition behaviors, we computed the heat capacity, shown in Fig. 5, which displays three anomalies for $J_3=0.4$ and only two for $J_3=1.2$. In the generalized XY model, the transition at $T_{\rm dw}$ is usually attributed to Ising-type domain walls [40]. In our case, the transition at $T_{\rm dw}$ is not driven by Ising-type domain walls and therefore is unlikely to be Ising. Instead, it is more consistent with a BKT transition: as shown in Fig. 5, the heat capacity exhibits a broad bump rather than a sharp peak at $T_{\rm dw}$. Within the quasi-long-range nematic phase, the correlation function follows a power law, $\langle \cos(\phi_i - \phi_j) \rangle \sim e^{-\langle (\phi_i - \phi_j)^2 \rangle/2} \sim |\mathbf{r}_i - \mathbf{r}_j|^{-\tilde{\eta}(T)}$, with $\tilde{\eta}(T_c) = 1/4$. Since $Q \sim e^{i2\phi}$, the corresponding critical exponent is $\eta = 4\tilde{\eta}$. At $T_{\rm nem}$, we indeed find $\eta = 1$, consistent with the proliferation of

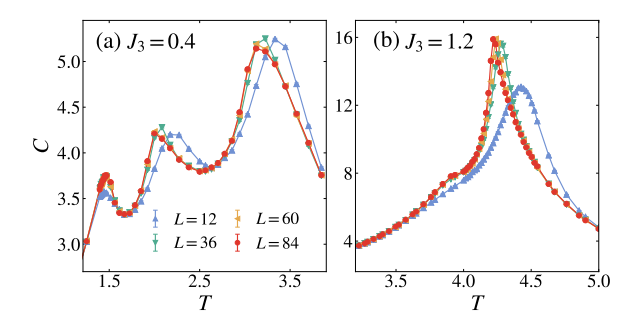


FIG. 5. The heat capacity for (a) $J_3 = 0.4$ and (b) $J_3 = 1.2$. The number of bumps indicates the number of transitions, which is three and two, respectively.

nematic vortices [61].

Conclusion.—To conclude, we have proposed a lattice model that realizes a nematic superconductor and hosts a rich set of vestigial phases, including charge-4e order and quasi-nematicity. The model provides a concrete lattice realization of the field-theoretic scenarios for melting multi-component superconductors into charge-4e states [9, 15, 16]. Unlike previous works, we demonstrate that the destruction of charge-4e order is driven by half superconducting vortices rather than $(\frac{1}{2}, \frac{1}{2})$ vortices, and, most strikingly, we identify a new quasi-nematic phase that intervenes between the nematic SC and charge-4e states, stabilized by domain-wall excitations.

Through theoretical analysis, we show that the sequence of transitions and vestigial orders arises from the proliferation of distinct topological defects, including half SC vortices, $(\frac{1}{2}, \frac{1}{2})$ vortices, integer nematic vortices, and domain-wall excitations. This picture is further corroborated by Monte Carlo simulations. Our results highlight the crucial role played by domain walls, in addition to various vortices, in shaping the vestigial phases of multicomponent superconductors. In terms of perspective, it will be interesting to explore how different types of superconducting domain walls and nematic domains affect the proliferation of fractional vortices and the phase diagram of systems with vestigial orders.

Acknowledgments: We thank Eduardo Fradkin, Shao-Kai Jian, Steve Kivelson, Zijian Wang, and Hao-Xin Wang for helpful discussions. This work is supported in part by the NSFC under Grant Nos. 12347107 and 12334003 (X.Z., Z.-Q.W., and H.Y.), MOSTC under Grant No. 2021YFA1400100 (H.Y.), and the New Cornerstone Science Foundation through the Xplorer Prize (H.Y.). The Flatiron Institute is a division of the Simons Foundation.

- superconductivity, Phys. Rev. 108, 1175 (1957).
- [2] S. A. Kivelson, V. J. Emery, and H. Q. Lin, Doped antiferromagnets in the weak-hopping limit, Phys. Rev. B 42, 6523 (1990).
- [3] G. Röpke, A. Schnell, P. Schuck, and P. Nozières, Fourparticle condensate in strongly coupled fermion systems, Phys. Rev. Lett. 80, 3177 (1998).
- [4] B. Doucot and J. Vidal, Pairing of cooper pairs in a fully frustrated josephson-junction chain, Phys. Rev. Lett. 88, 227005 (2002).
- [5] J. E. Moore and D.-H. Lee, Geometric effects on t-breaking in p + ip and d + id superconducting arrays, Phys. Rev. B **69**, 104511 (2004).
- [6] A. A. Aligia, A. P. Kampf, and J. Mannhart, Quartet formation at (100)/(110) interfaces of d-wave superconductors, Phys. Rev. Lett. 94, 247004 (2005).
- [7] C. Wu, Competing orders in one-dimensional spin-3/2 fermionic systems, Phys. Rev. Lett. 95, 266404 (2005).
- [8] W.-H. Ko, P. A. Lee, and X.-G. Wen, Doped kagome system as exotic superconductor, Phys. Rev. B 79, 214502 (2009).
- [9] E. Berg, E. Fradkin, and S. A. Kivelson, Charge-4e superconductivity from pair-density-wave order in certain high-temperature superconductors, Nat. Phys. 5, 830 (2009).
- [10] E. V. Herland, E. Babaev, and A. Sudbø, Phase transitions in a three dimensional $u(1) \times u(1)$ lattice london superconductor: Metallic superfluid and charge-4e superconducting states, Phys. Rev. B **82**, 134511 (2010).
- [11] Y.-Z. You, Z. Chen, X.-Q. Sun, and H. Zhai, Superfluidity of bosons in kagome lattices with frustration, Phys. Rev. Lett. 109, 265302 (2012).
- [12] J. Armaitis, R. A. Duine, and H. T. C. Stoof, Quantum rotor model for a bose-einstein condensate of dipolar molecules, Phys. Rev. Lett. 111, 215301 (2013).
- [13] Y.-F. Jiang, Z.-X. Li, S. A. Kivelson, and H. Yao, Charge-4e superconductors: A majorana quantum monte carlo study, Phys. Rev. B 95, 241103 (2017).
- [14] D. F. Agterberg, J. S. Davis, S. D. Edkins, E. Fradkin, D. J. Van Harlingen, S. A. Kivelson, P. A. Lee, L. Radzihovsky, J. M. Tranquada, and Y. Wang, The physics of pair-density waves: Cuprate superconductors and beyond, Annu. Rev. Condens. Matter Phys. 11, 231 (2020).
- [15] S.-K. Jian, Y. Huang, and H. Yao, Charge-4e superconductivity from nematic superconductors in two and three dimensions, Phys. Rev. Lett. 127, 227001 (2021).
- [16] R. M. Fernandes and L. Fu, Charge-4e superconductivity from multicomponent nematic pairing: Application to twisted bilayer graphene, Phys. Rev. Lett. 127, 047001 (2021).
- [17] M. Zeng, L.-H. Hu, H.-Y. Hu, Y.-Z. You, and C. Wu, High-order time-reversal symmetry breaking normal state, arXiv:2102.06158 (2021).
- [18] N. V. Gnezdilov and Y. Wang, Solvable model for a charge-4e superconductor, Phys. Rev. B 106, 094508 (2022).
- [19] P. Li, K. Jiang, and J. Hu, Charge 4e superconductor: A wavefunction approach, Sci. Bull. 69, 2328 (2024).
- [20] Y.-B. Liu, J. Zhou, C. Wu, and F. Yang, Charge-4e superconductivity and chiral metal in 45-twisted bilayer cuprates and related bilayers, Nat. Commun. 14, 7926 (2023).
- [21] Y.-M. Wu and Y. Wang, d-wave charge-4e superconductivity from fluctuating pair density waves,

^{*} yaohong@tsinghua.edu.cn

^[1] J. Bardeen, L. N. Cooper, and J. R. Schrieffer, Theory of

- arXiv:2303.17631 (2023).
- [22] M. Hecker, R. Willa, J. Schmalian, and R. M. Fernandes, Cascade of vestigial orders in two-component superconductors: Nematic, ferromagnetic, s-wave charge-4e, and d-wave charge-4e states, Phys. Rev. B 107, 224503 (2023).
- [23] M. O. Soldini, M. H. Fischer, and T. Neupert, Charge-4e superconductivity in a hubbard model, Phys. Rev. B 109, 214509 (2024).
- [24] A. Samoilenka and E. Babaev, Microscopic theory of electron quadrupling condensates, arXiv:2505.12542 (2025).
- [25] Z.-P. Sun and H.-Q. Lin, Emergence of diverse array of phases in an exactly solvable model, arXiv:2310.20306 (2023).
- [26] C. M. Varma and Z. Wang, Extended superconducting fluctuation region and 6e and 4e flux-quantization in a kagome compound with a normal state of 3q-order, arXiv:2307.00448 (2023).
- [27] L. Chirolli, A. Braggio, and F. Giazotto, Cooper quartets in interacting hybrid superconducting systems, Phys. Rev. Res. 6, 033171 (2024).
- [28] M. Hecker and R. M. Fernandes, Local condensation of charge-4e superconductivity at a nematic domain wall, Phys. Rev. B 109, 134514 (2024).
- [29] Y.-M. Wu, C. Murthy, and S. A. Kivelson, Possible sliding regimes in twisted bilayer wte₂, Phys. Rev. Lett. 133, 246501 (2024).
- [30] R. Ojajärvi, A. V. Chubukov, Y.-C. Lee, M. Garst, and J. Schmalian, Pairing at a single Van Hove point, npj Quantum Materials 9, 105 (2024).
- [31] Y. Verghis, D. Sedov, J. Weßling, P. P. Poduval, and M. S. Scheurer, Vestigial pairing from fluctuating magnetism and triplet superconductivity, arXiv:2510.02474 (2025).
- [32] I. Maccari, E. Babaev, and J. Carlström, Revisiting vestigial order in nematic superconductors: Gauge-field mechanisms and model constraints, arXiv:2505.11630 (2025).
- [33] L. Zhang, Y.-H. Zhang, and X.-Y. Song, Charge-4*e* anyon superconductor from doping SU(4)₁ chiral spin liquid, arXiv:2508.12370 (2025).
- [34] E. Huecker and Y. Wang, Vestigial d-wave charge-4e superconductivity from bidirectional pair density waves, arXiv:2510.05209 (2025).
- [35] J. Ge, P. Wang, Y. Xing, Q. Yin, A. Wang, J. Shen, H. Lei, Z. Wang, and J. Wang, Charge-4e and charge-6e flux quantization and higher charge superconductivity in kagome superconductor ring devices, Phys. Rev. X 14, 021025 (2024).
- [36] V. L. Berezinskii, Destruction of long range order in onedimensional and two-dimensional systems having a continuous symmetry group. I. Classical systems, Sov. Phys. JETP 32, 493 (1971).
- [37] J. M. Kosterlitz and D. J. Thouless, Ordering, metastability and phase transitions in two-dimensional systems, J. Phys. C Solid State Phys. 6, 1181 (1973).
- [38] J. M. Kosterlitz, The critical properties of the twodimensional xy model, J. Phys. C Solid State Phys. 7, 1046 (1974).
- [39] S. E. Korshunov, Possible splitting of a phase transition in a 2d xy model, JETP Lett. (Engl. Transl.) 41:5 (1985).
- [40] D. H. Lee and G. Grinstein, Strings in two-dimensional classical xy models, Phys. Rev. Lett. 55, 541 (1985).
- [41] D. B. Carpenter and J. T. Chalker, The phase diagram of a generalised xy model, J. Phys.: Condens. Matter 1,

- 4907 (1989).
- [42] F. C. Poderoso, J. J. Arenzon, and Y. Levin, New ordered phases in a class of generalized xy models, Phys. Rev. Lett. 106, 067202 (2011).
- [43] Y. Shi, A. Lamacraft, and P. Fendley, Boson pairing and unusual criticality in a generalized xy model, Phys. Rev. Lett. 107, 240601 (2011).
- [44] D. M. Hübscher and S. Wessel, Stiffness jump in the generalized xy model on the square lattice, Phys. Rev. E 87, 062112 (2013).
- [45] P. Serna, J. T. Chalker, and P. Fendley, Deconfinement transitions in a generalised xy model, J. Phys. A: Math. Theor. 50, 424003 (2017).
- [46] D. X. Nui, L. Tuan, N. D. Trung Kien, P. T. Huy, H. T. Dang, and D. X. Viet, Correlation length in a generalized two-dimensional xy model, Phys. Rev. B 98, 144421 (2018).
- [47] F.-F. Song and G.-M. Zhang, Hybrid berezinskiikosterlitz-thouless and ising topological phase transition in the generalized two-dimensional xy model using tensor networks, Phys. Rev. B 103, 024518 (2021).
- [48] F.-F. Song and G.-M. Zhang, Phase coherence of pairs of cooper pairs as quasi-long-range order of half-vortex pairs in a two-dimensional bilayer system, Phys. Rev. Lett. 128, 195301 (2022).
- [49] F.-F. Song and G.-M. Zhang, Phase coherence of charge-6e superconductors with a frustrated kagome xy antiferromagnet, Chin. Phys. Lett. 42, 037401 (2025).
- [50] D. F. Agterberg and H. Tsunetsugu, Dislocations and vortices in pair-density-wave superconductors, Nat. Phys. 4, 639 (2008).
- [51] M. H. Hamidian, S. D. Edkins, S. H. Joo, A. Kostin, H. Eisaki, S. Uchida, M. J. Lawler, E.-A. Kim, A. P. Mackenzie, K. Fujita, J. Lee, and J. C. S. Davis, Detection of a Cooper-pair density wave in Bi2Sr2CaCu2O8+x, Nature 532, 343 (2016).
- [52] S. Rajasekaran, J. Okamoto, L. Mathey, M. Fechner, V. Thampy, G. D. Gu, and A. Cavalleri, Probing optically silent superfluid stripes in cuprates, Science 359, 575 (2018).
- [53] W. Ruan, X. Li, C. Hu, Z. Hao, H. Li, P. Cai, X. Zhou, D.-H. Lee, and Y. Wang, Visualization of the periodic modulation of Cooper pairing in a cuprate superconductor, Nat. Phys. 14, 1178 (2018).
- [54] S. D. Edkins, A. Kostin, K. Fujita, A. P. Mackenzie, H. Eisaki, S. Uchida, S. Sachdev, M. J. Lawler, E.-A. Kim, J. C. S. Davis, and M. H. Hamidian, Magnetic field-induced pair density wave state in the cuprate vortex halo, Science 364, 976 (2019).
- [55] Z. Du, H. Li, S. H. Joo, E. P. Donoway, J. Lee, J. C. S. Davis, G. Gu, P. D. Johnson, and K. Fujita, Imaging the energy gap modulations of the cuprate pair-density-wave state, Nature **580**, 65 (2020).
- [56] H. Chen, H. Yang, B. Hu, Z. Zhao, J. Yuan, Y. Xing, G. Qian, Z. Huang, G. Li, Y. Ye, S. Ma, S. Ni, H. Zhang, Q. Yin, C. Gong, Z. Tu, H. Lei, H. Tan, S. Zhou, C. Shen, X. Dong, B. Yan, Z. Wang, and H.-J. Gao, Roton pair density wave in a strong-coupling kagome superconductor, Nature 599, 222 (2021).
- [57] K. Matano, M. Kriener, K. Segawa, Y. Ando, and G.-q. Zheng, Spin-rotation symmetry breaking in the superconducting state of CuxBi2Se3, Nat. Phys. 12, 852 (2016).
- [58] S. Yonezawa, K. Tajiri, S. Nakata, Y. Nagai, Z. Wang, K. Segawa, Y. Ando, and Y. Maeno, Thermodynamic ev-

- idence for nematic superconductivity in CuxBi2Se3, Nat. Phys. 13, 123 (2017).
- [59] Y. Cao, D. Rodan-Legrain, J. M. Park, N. F. Q. Yuan, K. Watanabe, T. Taniguchi, R. M. Fernandes, L. Fu, and P. Jarillo-Herrero, Nematicity and competing orders in superconducting magic-angle graphene, Science 372, 264 (2021).
- [60] Y.-B. Liu, J. Zhou, and F. Yang, Nematic superconductivity and its critical vestigial phases in the quasicrystal, Phys. Rev. Lett. 133, 136002 (2024).
- [61] See Supplementary Material (SM).
- [62] V. Gali, M. Hecker, and R. M. Fernandes, Critical nematic phase with pseudogaplike behavior in twisted bilayers, Phys. Rev. Lett. 133, 236501 (2024).
- [63] Here the nematic field ϕ is already disordered, so the string tension that confined half SC vortices vanishes. The destruction of charge-4e order is not driven by $(\frac{1}{2}, \frac{1}{2})$ vortices, since half SC vortices have lower energy; this is consistent with our Monte Carlo simulations.
- [64] Y. Liu, T. Wei, G. He, Y. Zhang, Z. Wang, and J. Wang, Pair density wave state in a monolayer high-Tc ironbased superconductor, Nature 618, 934 (2023).
- [65] H. Zhao, R. Blackwell, M. Thinel, T. Handa, S. Ishida,

- X. Zhu, A. Iyo, H. Eisaki, A. N. Pasupathy, and K. Fujita, Smectic pair-density-wave order in EuRbFe4As4, Nature **618**, 940 (2023).
- [66] A. Aishwarya, J. May-Mann, A. Raghavan, L. Nie, M. Romanelli, S. Ran, S. R. Saha, J. Paglione, N. P. Butch, E. Fradkin, and V. Madhavan, Magnetic-fieldsensitive charge density waves in the superconductor UTe2, Nature 618, 928 (2023).
- [67] R. H. Swendsen and J.-S. Wang, Nonuniversal critical dynamics in monte carlo simulations, Phys. Rev. Lett. 58, 86 (1987).
- [68] U. Wolff, Collective monte carlo updating for spin systems, Phys. Rev. Lett. 62, 361 (1989).
- [69] K. Binder, Critical properties from monte carlo coarse graining and renormalization, Phys. Rev. Lett. 47, 693 (1981).
- [70] H. Weber and P. Minnhagen, Monte carlo determination of the critical temperature for the two-dimensional xy model, Phys. Rev. B 37, 5986 (1988).
- [71] Y.-D. Hsieh, Y.-J. Kao, and A. W. Sandvik, Finite-size scaling method for the berezinskii–kosterlitz–thouless transition, J. Stat. Mech.: Theory Exp. 2013 (09), P09001.

SUPPLEMENTAL MATERIALS

Landau free energy

The coupling term involving the fields θ_0 , θ , and ϕ in the free energy is given by:

$$\mathcal{F} = \frac{g}{2} \Delta_0^2 \Delta_+^* \Delta_-^* + \frac{g_3}{4} \Delta_0 \Delta_+ (\Delta_-^*)^2 + \frac{g_3}{4} \Delta_0 \Delta_- (\Delta_+^*)^2 + \frac{g_6}{2} (\Delta_+ \Delta_-^*)^3 + \text{h.c.}$$

$$= g|\Delta_0|^2 |\Delta_\pm|^2 \cos(2\theta_0 - 2\theta) + \frac{g_3}{2} |\Delta_0| |\Delta_\pm|^3 \cos(\theta_0 - \theta + 3\phi)$$

$$+ \frac{g_3}{2} |\Delta_0| |\Delta_\pm|^3 \cos(\theta_0 - \theta - 3\phi) + g_6 |\Delta_\pm|^6 \cos(6\phi)$$

$$= g|\Delta_0|^2 |\Delta_\pm|^2 \cos(2\theta_0 - 2\theta) + g_3 |\Delta_0| |\Delta_\pm|^3 \cos(\theta_0 - \theta) \cos(3\phi) + g_6 |\Delta_\pm|^6 \cos(6\phi)$$

Note that the representation $\Delta_{\pm} = |\Delta_{\pm}|e^{i(\theta \pm \phi)}$ exhibits a \mathbb{Z}_2 gauge redundancy under the transformations $\theta \to \theta + \pi$ and $\phi \to \phi + \pi$. Consequently, a term like $g_3 \cos(3\phi)$ cannot appear independently in the free energy; it must be coupled with a θ -dependent term to ensure gauge invariance. As discussed in the main text, the $\cos(6\phi)$ term becomes irrelevant at a temperature $T \sim \frac{4T_{\text{nem}}}{9}$, which is lower than $T'_{\text{nem}} \simeq T_{\text{dw}}$.

The transition from Phase I to Phase II corresponds to the disordering of the Δ_0 field. In other words, as the temperature increases past $T_{\rm dw}$, the \mathbb{Z}_2 symmetry the Δ_0 field is restored, and the \mathbb{Z}_6 symmetry of the ϕ field is enlarged to a U(1) symmetry. Consequently, the uniform charge-2e component vanishes, and the nematic order transitions into a quasi-long-range order.

The coupling between Δ_0 and Δ_{\pm} can also be understood in the context of PDW superconductivity. At the x=1/8 doping level in $\text{La}_{2-x}\text{Ba}_x\text{CuO}_4$, there is experimental signature of a transition from PDW with a uniform superconducting component to pure PDW superconductivity, which is related to the disordering of the Δ_0 field, similar to the case here. However, there is no anisotropic coupling to Δ_0 in PDW system, so in that case, the transition resembles a \mathbb{Z}_2 transition.

The fitting results

For $J_3 \leq 0.8$, there is a universal jump in the superfluid stiffness ρ at the BKT transition induced by half vortices proliferation, and the stiffness is related to the transition temperature T_{4e} by the equation $\rho = \frac{8}{\pi}T_{4e}$. To determine

the transition temperature at the thermodynamic limit, the fitting function $T^*(L) = T_{4e}(\infty) + \frac{a}{\ln^2(bL)}$ is applied, where L is the system size. For $J_3 \geq 1.0$, the superfluid stiffness no longer exhibits the universal jump at $\rho = \frac{8}{\pi}T_c$, but instead falls between $\rho = \frac{8}{\pi}T_c$ and $\rho = \frac{2}{\pi}T_c$. In this regime, the relation $\rho = \frac{2}{\pi}T_{4e}$ is used for fitting, which lies below the jump and can be extrapolated to obtain the correct transition temperature T_{4e} . In this case, the transition temperature is determined using the general function $T^*(L) = T_{4e}(\infty) + b/L^x$. As for the dimensionless quantities Binder Cumulants and the RG invariant ratio (e.g. the complementary results for $J_3 = 1.2$ as shown in Fig. S1), the crossing points of the data with size L and L+6 are first obtained. Then, the finite-size extrapolation is applied with the power-law form $T_c(L) = T_c(\infty) + b/L^x$. All the fitting results are summarized in Tab. S1.

TABLE S1. The transition temperatures with different values of J_3 are determined from different physical quantities. The stiffness ρ is the superfluid stiffness, which exhibits a discontinuity at T_{4e} . The U_{4e} , U_{2e} , and U_n are the Binder cumulants of uniform charge-4e, charge-2e, and nematic orders. R_n is the RG-invariant ratio of nematic order. T_{dw} , T_{nem} , and T_{4e} are related to the transition temperatures from phase I to II, II to III, and III to IV, respectively. T'_{nem} is the transition from nematic long-range order to quasi-long-range order, which coincides with T_{dw} .

\overline{T}	J_3	0	0.4	0.6	0.8	1	1.2	1.4	1.8
T_{4e}	ρ	2.6597(7)	2.7971(11)	2.9915(6)	3.2865(2)	3.763(3)	4.149(8)	4.555(9)	5.277(8)
T_{4e}	U_{4e}	2.678(8)	2.849(3)	3.01(4)	3.25(8)	3.72(6)	4.123(5)	4.493(5)	5.270(5)
$T_{ m dw}$	U_{2e}	_	1.59(4)	2.28(3)	2.93(4)	3.51(4)	4.05(3)	4.47(1)	5.268(5)
T_{nem}	U_n	_	1.87(2)	2.620(6)	3.14(8)	3.75(1)	4.15(4)	4.55(5)	5.28(3)
$T'_{\rm nem}$	R_n		1.59(1)	2.30(1)	2.936(4)	3.52(2)	4.000(3)	4.459(8)	5.269(2)

As we can see, the transition temperatures obtained from the spin stiffness ρ are in close agreement with those from U_{4e} for all J_3 , and also consistent with the results obtained from U_n within numerical error for $J_3 > J_3^*$, where $0.8 < J_3^* < 1.0$ is the tri-critical point. The transition points obtained from U_{2e} also coincide with R_n within numerical error for all J_3 .

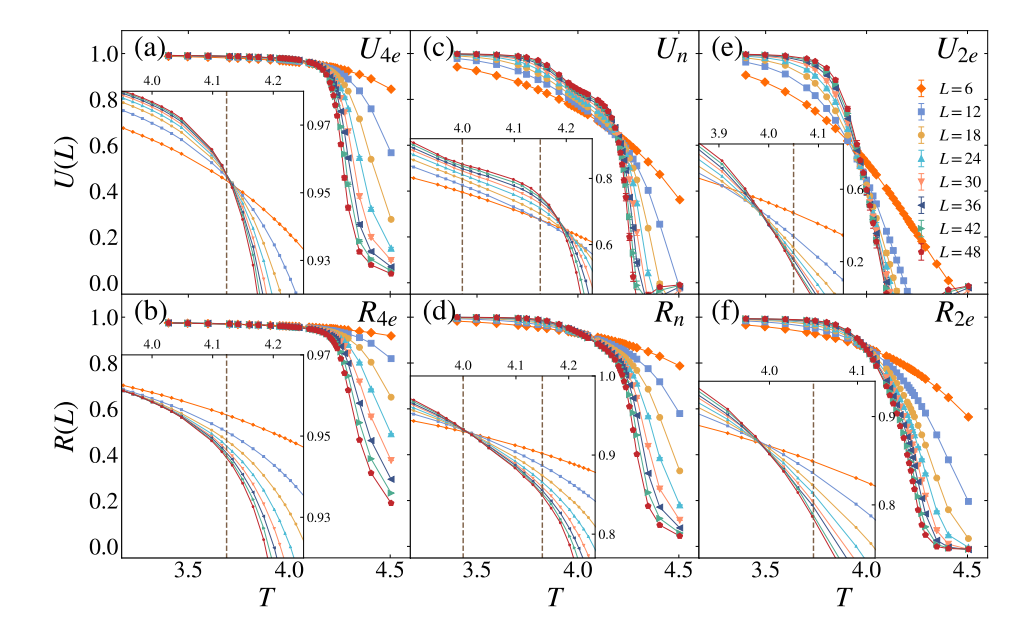


FIG. S1. The plot of Binder cumulants U(L) and the RG-invariant ratio R(L) for the different orders at $J_3=1.2$. The insets depict a close-up view of the transition points. (a)-(b) correspond to the charge-4e order, where the dashed line denotes the transition temperature $T_{4e}=4.123$. (c)-(d) represent the nematic order, with the dashed lines indicating the transition temperatures $T_{\text{nem}}=4.15$ and $T'_{\text{nem}}=4.0$. (e)-(f) show the uniform charge-2e order, where the dashed line denotes the transition temperature $T_{\text{dw}}=4.05$.

The critical exponents η

In the quasi-long range order phase, the magnetization satisfies $\ln(m^2) \sim -\eta \ln(L) + \text{const.}$ where $m^2 = \frac{1}{N^2} \langle |\sum_i \Delta_{2e}(\mathbf{r}_i)|^2 \rangle$ for the charge-2e case, and is defined analogously for the charge-4e and nematic order parameters.

We apply the linear fitting to the data with the four largest sizes $L=30\sim48$ and get the exponents η as follows.

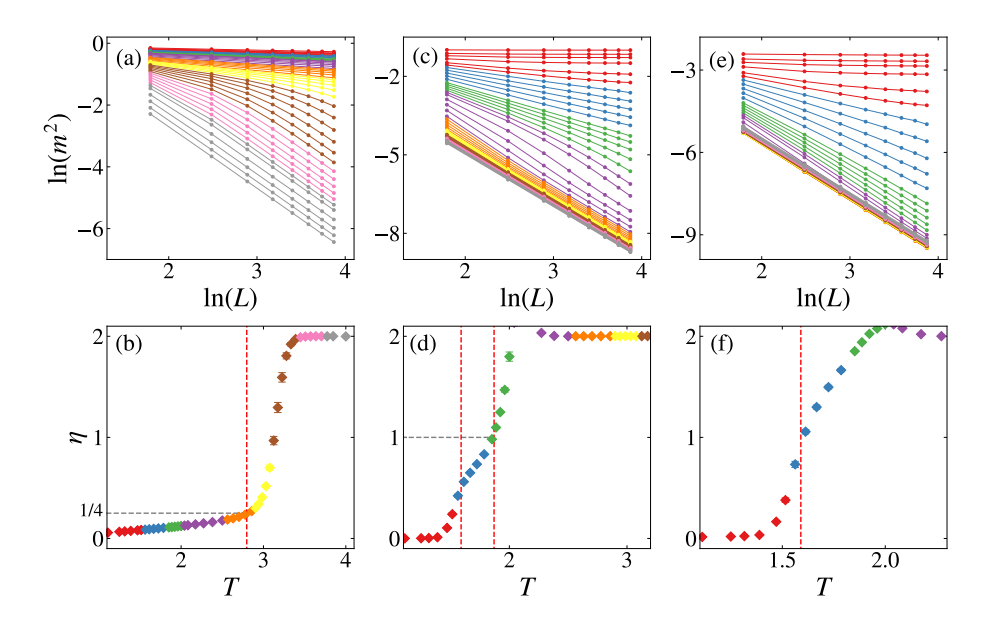


FIG. S2. The plot of $\ln(m^2)$ v.s. $\ln(L)$ and the critical exponents η v.s. T for $J_3=0.4$, where m^2 is defined with (a-b) charge-4e, (c-d) nematic, and (e-f) charge-2e order parameters. The colors in (a), (c), and (e) represent different temperatures as specified in (b), (d), and (f). The red dashed lines in (b), (d), and (f) denote the transition points T=2.7971, (1.87, 1.59), and 1.59.

For $J_3 = 0.4$, the behavior of the critical exponent η as a function of temperature is shown in Fig. S2 (b). As the temperature increases, η increases slowly until it reaches the BKT transition temperature, where the value of $\eta_c = 1/4$ is consistent with the $(\frac{1}{2}, 0)$ vortex proliferation (vortex for charge-4e order parameters).

The critical exponent η for the nematic order shows a two-step transition behavior, as shown in Fig. S2(d). It is close to 0 at T<1.59 and converges to 2 at T>1.87. When 1.59 < T < 1.87, the critical exponent η increases slowly with the temperature and indicates the quasi-long range order phase. At T=1.87, η is very close to 1, which is consistent with nematic vortex proliferation. As mentioned in the main text, the two elementary order parameters are $\Delta_{\pm} = |\Delta_{\pm}|e^{i\theta\pm\phi}$, and the nematic order parameter $Q \sim \Delta_{+}\Delta_{-}^{*} \sim e^{i2\phi}$ is only related to the nematic field ϕ . In the nematic quasi-long range order phase, the correlation function has a power law behavior $\langle \cos(\phi_{i}-\phi_{j})\rangle \sim e^{-\langle(\phi_{i}-\phi_{j})^{2}\rangle/2} \sim |\vec{R}_{i}-\vec{R}_{j}|^{-\tilde{\eta}(T)}$ with $\tilde{\eta}(T_{c})=1/4$. Since $Q\sim e^{i2\phi}$, the critical exponent η_{c} should be four times larger here, which is equal to 1.

For $J_3 > J_3^*$, both nematic and charge-4e quasi-long-range orders vanish simultaneously in a direct transition driven by $(\frac{1}{2}, \frac{1}{2})$ vortex proliferation. Results for $J_3 = 1.2$ are shown in Fig. S3. The critical exponents η for the charge-4e and nematic order parameters follow trends similar to those for $J_3 < J_3^*$, but deviate from the expected values $(\eta = 1/4$ for charge-4e and $\eta = 1$ for nematic). These deviations are natural consequences of $(\frac{1}{2}, \frac{1}{2})$ vortex proliferation.

1

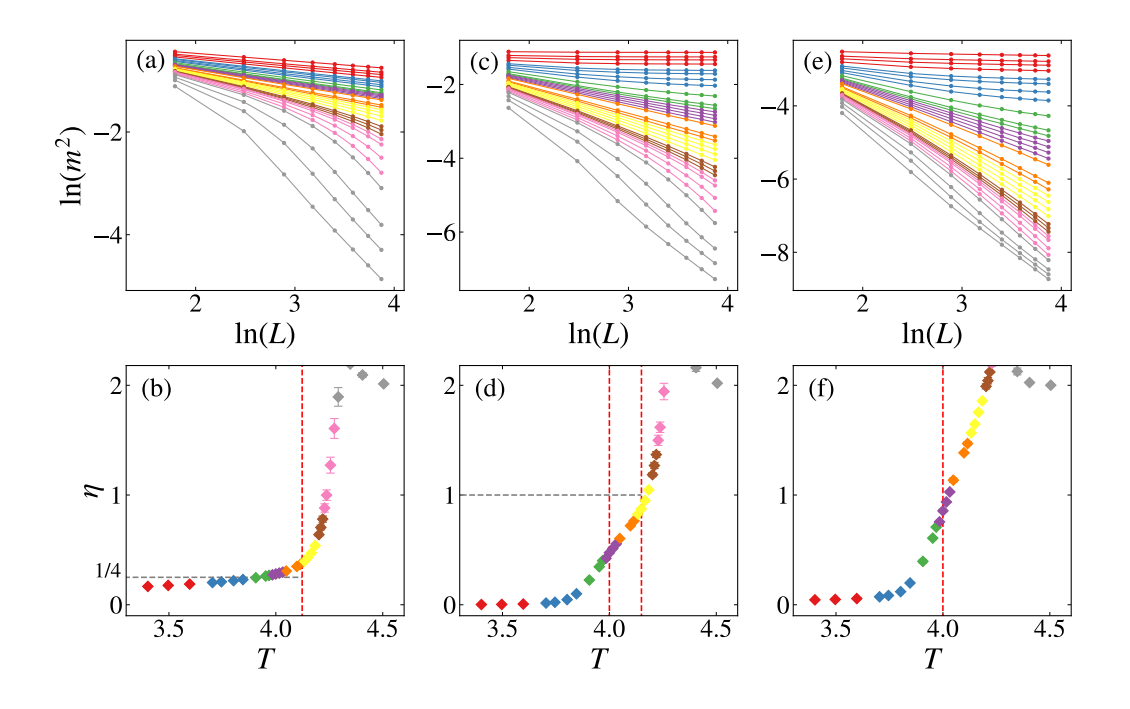


FIG. S3. The plot of $\ln(m^2)$ v.s. $\ln(L)$ and the critical exponents η v.s. T for $J_3=1.2$, where m^2 is defined with (a-b) charge-4e, (c-d) nematic, and (e-f) charge-2e order parameters. The colors in (a), (c), and (e) represent different temperatures as specified in (b), (d), and (f). The red dashed lines in (b), (d), and (f) denote the transition points T=4.123, (4.15,4.0), and 4.0.